Clinical & Experimental Immunology
The Journal of Translational Immunology

Clinical and Experimental Immunology ORIGINAL ARTICLE doi: 10.1111/cei.13410

Chemical chaperones reverse early suppression of regulatory circuits during unfolded protein response in B cells from common variable immunodeficiency patients

D. Bhatt,* R. C. Stan ,*† R. Pinhata,* M. Machado,* S. Maity,‡ C. Cunningham-Rundles,§ C. Vogel‡ and M. M. de Camargo *

*Department of Immunology, University of São Paulo, São Paulo, Brazil, †Department of Proteomics and Structural Biology, Cantacuzino Military Medical Research Development National Institute, Bucharest, Romania, ‡Center for Genomics and Systems Biology, New York University, and §Department of Medicine, Allergy & Immunology, Mount Sinai Medicine School, New York, NY.

Accepted for publication 15 December 2019

Correspondence: M. M. de Camargo, Instituto de Ciências Biomédicas, USP Edifício Biomédicas IV, Deptamento de Imunologia, Avenida Prof. Lineu Prestes, 1730 CEP 05508-900, Cidade Universitária São Paulo, SP, Brazil.
E-mail: mmcamar@usp.br

Summary

B cells orchestrate pro-survival and pro-apoptotic inputs during unfolded protein response (UPR) to translate, fold, sort, secrete and recycle immunoglobulins. In common variable immunodeficiency (CVID) patients, activated B cells are predisposed to an overload of abnormally processed, misfolded immunoglobulins. Using highly accurate transcript measurements, we show that expression of UPR genes and immunoglobulin chains differs qualitatively and quantitatively during the first 4 h of chemically induced UPR in B cells from CVID patients and a healthy subject. We tested thapsigargin or tunicamycin as stressors and 4-phenylbutyrate, dimethyl sulfoxide and tauroursodeoxycholic acid as chemical chaperones. We found an early and robust decrease of the UPR upon endoplasmic reticulum (ER) stress in CVID patient cells compared to the healthy control consistent with the disease phenotype. The chemical chaperones increased the UPR in the CVID patient cells in response to the stressors, suggesting that misfolded immunoglobulins were stabilized. We suggest that the AMP-dependent transcription factor alpha branch of the UPR is disturbed in CVID patients, underlying the observed expression behavior.

Keywords: chaperones, common variable immunodeficiency, human B cells, regulatory circuits, unfolded protein response

Introduction

Activated B lymphocytes have to respond to increased rates of protein translation, folding and secretion without activating cell death related to stress of the endoplasmic reticulum (ER) [1,2]. Unfolded proteins are sensed by three ER resident sensors: serine/threonine–protein kinase/endoribonuclease IRE1α (IRE1α), eukaryotic translation initiation factor 2–alpha kinase 3 (PERK) and cyclic AMP-dependent transcription factor alpha ATF-6α (ATF6α), that are responsible for initiating the unfolded protein response (UPR) via three branches.

ATF6α activates transcription of several ER chaperones and co-chaperones, including binding immunoglobulin protein (BiP), also known as glucose-regulated protein 78 (GRP78, kDa or HSPA5), GRP94, GRP170, calreticulin (CALR) and ERdj3 (DnaJ homolog subfamily B member 11) [3,4]. ATF6α also contributes to transcription of ER degradation-enhancing alpha-mannosidase-like protein 1 (EDEM1) and C/EBP-homologous protein, or DDIT3 for DNA damage-inducible transcript 3 protein (CHOP), a multi-functional transcription factor involved in ER stress responses and apoptosis.

IRE1α is a dual protein kinase–endoribonuclease that, among other functions, splices *Xbp1* mRNA, resulting in the active form of X-box binding protein 1 (XBP1) and inducing the expression of co-chaperone ERdj4 (DnaJ homolog subfamily B member 9). Through its endoribonuclease domain, IRE1α performs regulated IRE1-dependent decay of mRNA (RIDD), inhibiting translation of several mRNA targets, including XBP1 and apoptosis effector death receptor 5 [DR5 or tumor necrosis factor (TNF) receptor superfamily member 10B] [5]. PERK activation increases the translation rate of cyclic ATF4, which co-regulates transcription of *Hspa5* and *Chop* [6].

Evidence suggests that plasma cells present a 'physiological' UPR, contrasting to a canonical, stress-induced UPR [7–9]. In B cells, an early expansion of both the metabolic capacity of the ER and the secretory machinery must be achieved to accommodate the massive production of

immunoglobulins that follows their activation [7,10,11]. Unsurprisingly, immunoglobulin chains folding and assembly therefore depend upon several ER chaperones and co-chaperones under the control of transcription factor ATF6α, such as HSPA5/BiP [12,13], GRP94 [14], GRP170 [15] and ERdj3 [16]. Spliced XBP1 is required for antibody production *in vivo*, as well as terminal differentiation of B cells into plasma cells [17]. In mouse, XBP1 is induced by interleukin (IL)-4, a cytokine involved in survival of B cells, and induces expression of IL-6, a cytokine involved in plasma cell differentiation. Accumulation of immunoglobulin (Ig)M precedes *Xbp1* mRNA splicing by IRE1α in these cells, and thus UPR is considered a required step for complete B cell differentiation [10].

Common variable immunodeficiency (CVID) is a clinically and genetically heterogeneous group of disorders where patients present hallmark loss of at least two immunoglobulin isotypes (IgG and IgA and/or IgM) and impaired specific antibody production [18,19]. CVID are the most prevalent cause of hypogammaglobulinemia in adults, affecting ≥ 1 : 25 000 [20]. The molecular defects underlying this hypogammaglobulinemia have different origins, including defective molecules of B and/or T lymphocytes such as inducible T cell stimulator (ICOS) [21], transmembrane activator and calcium-modulator and cyclophilin ligand interactor (TACI) [22], CD19 [23], B cell activating factor receptor (BAFF-R) [24], CD20 [25] and CD81 [26]. However, more than 80% of the CVID patients present none of the known defects [27,28]. Previously, we have described a CVID patient whose delayed activation of the UPR correlated with accumulation of IgM chains inside the ER [29]. Considering that both pro-survival and pro-apoptotic pathways are simultaneously activated by the UPR, we aimed to explore the initial hours of the UPR in B cells from CVID patients and compare the results to a healthy donor's UPR. We hypothesized that quanti- and/or qualitatively distinct regulatory circuits occur in the initial hours of UPR in CVID patients' cells that would predispose these cells to abnormal processing of the misfolded immunoglobulin overload following B cell activation. In turn, this would lead to failure at properly folding and secreting immunoglobulins.

Here, we obtained rare B cell samples from two CVID patients and a healthy donor and conducted controlled experiments analyzing the early UPR with and without the presence of chemical chaperones. As ER stressors we used thapsigargin (Tg), a blocker of SERCA-mediated uptake of calcium into the ER, and thus considered a quick activator of the UPR [30]; and tunicamycin (Tm) that inhibits N-glycosylation, and is thus considered a slower inducer of misfolded protein accumulation [31]. As exogenous chaperones we used dimethylsulfoxide (DMSO), phenylbutyrate (PBA) and tauroursodeoxycholic acid (TUDCA). DMSO is a polar aprotic osmolyte commonly used as a solvent that also has a global effect on stabilization of protein folding and scavenging properties against reactive oxygen species [32]. DMSO is used clinically as an anti-inflammatory agent in the treatment of endotoxemia in horses [33]. 4-Phenylbutyrate (4-PBA) is a short-chain fatty acid that acts as a hydrophobic chaperone. PBA is Food and Drug Administration (FDA)-approved for use in patients with urea-cycle disorders, but holds potential benefits for several protein folding diseases: type II diabetes mellitus [34], Alzheimer's disease [35] and Parkinson's disease [36]. TUDCA is an acidic steroid (bile acid) synthesized from cholesterol in the liver that presents anti-amyloidogenic activity and modulates apoptotic pathways [37,38]. TUDCA is a taurine conjugate of ursodeoxycholic acid (UDCA), an FDA-approved bile acid for treatment of primary biliary cirrhosis [39].

Our results provide first evidence that CVID patients present an early and robust down-regulation of the regulatory circuits involved in UPR upon ER stress. Our data also show that chemical chaperones are promising therapeutic tools in reversing such inhibitory events. We provide models with specific predictions for mechanisms leading to hypogammaglobulinemia in CVID patients.

Material and methods

EBV-immortalization of B cells

One peripheral blood sample was obtained from one adult healthy donor (identified as 'C') and two adult patients with CVID ('P1' and 'P2') after informed and signed consent. Peripheral blood mononuclear cells (PBMC) were obtained by centrifugation of the blood sample over Isolymph® gradient (GE Healthcare, Chicago, IL, USA). PBMC were harvested at the interface, washed three times in phosphate-buffered saline (PBS) and immediately processed. B cells were isolated using magnetic beads (MACS; Miltenyi Biotech, San Diego, CA, USA), according to the manufacturer's protocol. Immortalization of B cells was performed according to standard protocol using Epstein–Barr virus (EBV) [40]. All study protocols and consent were approved by the University of São Paulo Institutional Human Research Ethics Committee (CEPSH.090.12) and by the Mount Sinai Institutional Review Board. Clinical data on these donors can be found in Supporting information, Table S1.

Cell culture of immortalized EBV-B cells and experimental set-up

EBV-immortalized B (EBV-B) cells were cultured in RPMI-1640 GlutaMAX media containing penicillin–streptomycin and 10% heat-inactivated fetal bovine serum (all from ThermoFisher Scientific, Fremont, CA, USA) at 37°C and 5% CO_2. Cells were split every 3 days, and harvested for

13652249, 2020, 1, Downloaded from https://onlinelibrary.wiley.com/doi/10.1111/cei.13410 by Universiteitsbibliotheek, Wiley Online Library on [04/08/2025]. See the Terms and Conditions (https://onlinelibrary.wiley.com/terms-and-conditions) on Wiley Online Library for rules of use; OA articles are governed by the applicable Creative Commons License

experiments between the third and tenth split. Cell viability was determined by Trypan blue staining using an automatic counter Countess II (ThermoFisher Scientific). The cells were plated as triplicates at 3×10^5 cells/well (96 round-bottomed wells per plate) in media containing chemical chaperones (final concentrations were 1 mM PBA, 5 mM TUDCA or 1 mM DMSO (all from Sigma, St Louis, MO, USA) and/or ER stressors at final concentrations of 1 μM Tg or 10 μg/ml Tm (both from Sigma). Cells were stimulated for 1, 2, 3 and 4 h or left untreated. Refer to Fig. 1b for the experimental design.

Cell growth quantification

EBV-B cells were plated as duplicates in parallel plates and kept at 37°C and 5% CO_2 for up to 11 days to characterize their growth pattern. Incorporation of bromodeoxyuridine (BrdU) was measured using the Cell Proliferation Biotrak enzyme-linked immunosorbent assay (ELISA) system (GE Healthcare), according to the manufacturer's instructions. Samples were assayed in technical duplicates, and readings were pooled for averaging and standard deviation (s.d.) calculation.

Microscopy

One million EBV-B cells were washed twice in cold PBS and fixed with cold acetone for 5 min. Cells were blocked with T-PBS–1% bovine serum albumin (BSA)–22·3 mg/ml glycine at room temperature for 30 min, followed by staining with anti-human immunoglobulin (Ig)M (Abcam, Cambridge, UK; ab772) for 1 h at room temperature. Secondary staining used anti-mouse IgG-Alexa Fluor 488 (Abcam; ab150109) for 1 h at room temperature in the dark. Images were acquired in an In Cell Analyzer 2200 (GE Healthcare).

Transcript quantification

For quantification of specific transcripts of interest, we used a high-throughput platform based on TaqMan technology [Applied Biosystems, Carlsbad, CA, USA; TaqMan OpenArray real-time–polymerase chain reaction (RT–PCR) system; ThermoFisher Scientific]. EBV-B cells were seeded in quadruplicate plates so that during the processing of a given time-point only one plate was manipulated at room temperature, while the remaining plates were left in the incubator undisturbed. All treatments and time-points were performed in triplicate. Samples containing 3×10^5 EBV-B cells that received treatments with ER stressors and/or chemical chaperones for 0, 1, 2, 3 or 4 h were harvested in RNAlater (ThermoFisher Scientific) and kept at −20°C until processing. Total RNA was isolated using Purelink Mini (ThermoFisher Scientific) and kept at −80°C until further processing. Purified RNA was qualified and quantified by spectrometry in a Nanodrop and by fluorimetry in a Qubit, respectively (both equipments by ThermoFisher Scientific). When needed, RNA was precipitated by standard protocol using sodium acetate, glycogen and isopropanol. All RNA samples were normalized to 30 ng/μl before proceeding. cDNA was generated using 300 ng of total RNA and the high-capacity RNA-to-cDNA kit (ThermoFisher Scientific), following the manufacturer's instructions. cDNA was kept at −20°C until further processing. Thirty-three nL of PCR mixture (TaqMan OpenArray RT–PCR master mix, ThermoFisher Scientific) were loaded into custom-made TaqMan OpenArray slides by an automated system (Accufill; ThermoFisher Scientific) and amplified in triplicate reactions for quantification of specific transcripts using a QuantStudio 12K Flex RT–PCR System (ThermoFisher Scientific) for up to 40 cycles. Images of the microarray slides before and after amplification were visually inspected to ensure homogeneous amplification of wells. TaqMan OpenArray primers were custom-made by ThermoFisher Scientific, and validated previously by the manufacturer for specificity and efficiency of amplification. Genes access numbers can be found in Supporting information, Table S2. *Xbp1* primers amplified a 60 bases region on the exons 3 and 4 boundary, thus amplifying both the unspliced and spliced forms of the transcripts.

Quality control and data analysis

Amplification curves (nine curves per gene in each treatment condition) were visually inspected for slope, fluorescence intensity, cathode-ray tubes (CRTs), outliers, aberrant replicates and for stability of *Gapdh* expression. Each curve was contrasted individually against the quality data of its original RNA. Target DC_q values were normalized against *Gapdh* DC_q levels. Replicates were averaged and filtered for standard error (s.e.) < 0·5 for removal of low-abundance measurements. A ratio of treated/untreated was calculated, $\log_2$-transformed and a *t*-test was applied. Only those ratios whose s.e. were < 0·5 and that were significantly different ($P \leq 0{\cdot}05$) from untreated controls in at least two time-points were considered relevant. These rules resulted in a high-confidence data set. Heat-maps were built using treated/untreated values and boundaries of ± 0·58 (on log base 2 scale).

Network reconstruction

Regulatory circuits were built using BioTapestry version 7.1 software [41,42]. Networks show only those elements assayed in this study. For canonical representation of the UPR refer to Fig. 1c. Inputs and outputs of indicated genes are color-coded according to their upstream origin (yellow for ATF6, red for PERK, blue for IRE1a and green for sXBP1). Orange lines indicate those elements whose expression depends on inputs from both ATF6 and PERK pathways. Linkages substantiated by *cis*-regulatory data are

13652249, 2020, 1, Downloaded from https://onlinelibrary.wiley.com/doi/10.1111/cei.13410 by Universiteitsbibliotheek, Wiley Online Library on [04/08/2025]. See the Terms and Conditions (https://onlinelibrary.wiley.com/terms-and-conditions) on Wiley Online Library for rules of use; OA articles are governed by the applicable Creative Commons License

indicated by diamonds colored according to the strength of the experimental evidence: blue diamonds for expression studies using gain/loss of function, pink diamonds for binding affinity assays and orange diamonds for promoter analysis *in vivo*. A green bar represents post-transcriptional modification of *Xbp1* mRNA. A yellow bar represents post-translational modification of ATF6 protein. # (OR) and & (AND) are Boolean rules governing input elements in specific promoters; bold gene = active expression; bold gene + thick line = up-regulated expression compared to untreated control; gray gene + gray line = down-regulated expression compared to untreated control. For visualization

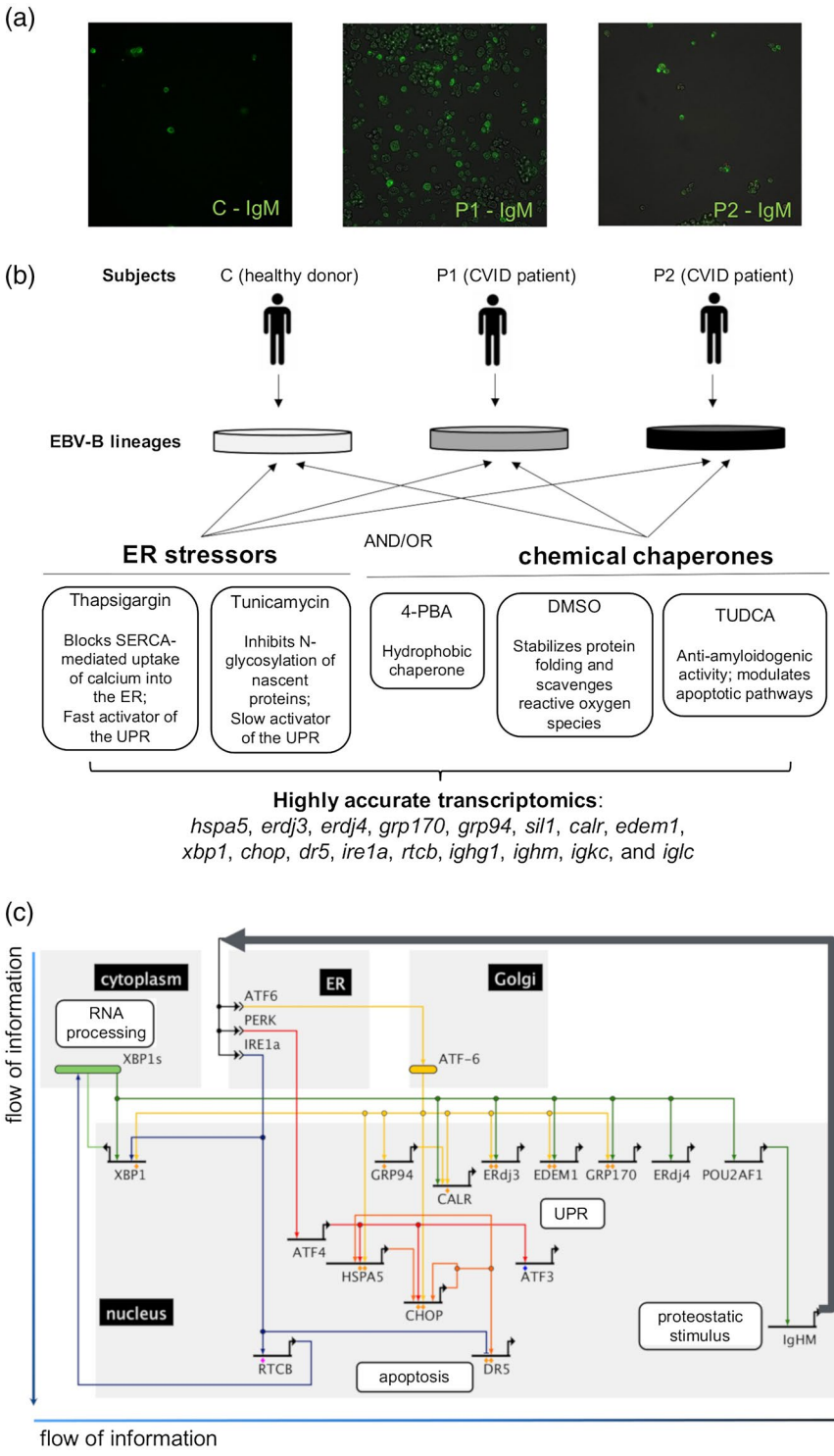

13652249, 2020, 1, Downloaded from https://onlinelibrary.wiley.com/doi/10.1111/cei.13410 by Universiteitsbibliotheek, Wiley Online Library on [04/08/2025]. See the Terms and Conditions (https://onlinelibrary.wiley.com/terms-and-conditions) on Wiley Online Library for rules of use; OA articles are governed by the applicable Creative Commons License

Fig. 1. Defective immunoglobulin folding in common variable immunodeficiency (CVID) patients. (a) Membrane-bound IgM (green) expression by fluorescence microscopy. Healthy donor (c) cells are shown in the left panel and patients' cells (P1 and P2, middle and right panels, respectively) are shown at ×100 magnification. (b) Schematic illustration of the experimental design. Thapsigargin (Tg) and tunicamycin (Tm) elicit endoplasmic reticulum (ER), triggering three branches of the unfolded protein response (UPR). Exogenous chemical chaperones act upon different effector elements of the UPR, counterbalancing pro-apoptotic and deleterious pathways. All treatments were performed in biological triplicates. mRNA abundances for 13 UPR genes and four proteostatic stimuli were measured (in technical triplicates) using Taqman in an open array platform. Genes with significant ($P < 0{\cdot}05$ or less) expression changes were extracted. (c) Canonical regulatory network for the UPR in mature human B cells. This network shows only those elements assayed in this study. This regulatory circuit was inferred from current literature and considers only immunoglobulin (Ig)M as proteostatic stimulus for clarity. Inputs and outputs of indicated genes are color-coded according to their upstream origin [yellow for activating transcription factor 6 (ATF6), red for eukaryotic translation initiation factor 2-alpha kinase 3 (PERK), blue for serine/threonine-protein kinase/endoribonuclease (IRE1α) and green for spliced X-box binding protein 1 (sXBP1)]. Orange lines indicate elements whose expression depends on inputs from both ATF6 (yellow) and PERK (red) pathways. Linkages substantiated by *cis*-regulatory data are indicated by diamonds colored according to strength of the experimental evidence: blue diamonds for expression studies using gain/loss of function, pink diamonds for binding affinity assays and orange diamonds for promoter analysis *in vivo*. A green bar represents post-transcriptional modification of *Xbp1* mRNA. A yellow bar represents post-translational modification of ATF6 protein. # (OR) and & (AND) are Boolean rules governing input elements in specific promoters. Bold gene = active expression. Bold gene + thick line = up-regulated expression compared to untreated control. Gray gene + gray line = down-regulated expression compared to untreated control.

of each patient's experimental regulatory network, refer to Supporting information, Movies (a–g) for average (CVID patients minus healthy control), (h–n) for healthy control, (o–u) for patient P1 and (v–y) for patient P2.

Data availability

All transcriptomics data generated in this study have been deposited in NCBI's Gene Expression Omnibus (GEO Series Accession number GSE126201).

Results

EBV immortalization did not inhibit surface IgM expression of mature B cells from CVID patients

We tested if infection with EBV inhibited surface IgM expression by B cells from one healthy donor (C) and two CVID patients (P1 and P2). Expression of monomeric IgM in the B cell surface was heterogeneous in CVID patients (Fig. 1a, middle and right panels). Healthy donor EBV-B cells, in contrast, were uniformly positive with distinct surface staining for IgM (Fig. 1a, left panel). Both patients presented lower levels of serum IgG and IgM at the time of CVID diagnosis despite the number of circulating B cells being within the normal range (Supporting information, Table S1). EBV-B cells from CVID patients presented lower growth rates over 11 days (Supporting information, Fig. S1a, middle and right panels) when compared to EBV-B from a healthy donor (Supporting information, Fig. S1a, left panel), consistent with *ex-vivo* data from the same patients (Supporting information, Table S1).

Chemical chaperones have a positive effect on the expression of most UPR targets

To investigate the impact of ER stressors and chaperones on first hours of the response, we subjected these EBV-B cell lines to a time–course experiment. Cells were left untreated or stressed with 1 μM Tg or 10 μg/ml Tm in the presence or absence of 1 mM 4-PBA, 1 mM DMSO or 5 mM TUDCA. Cells were assayed at time-points 0, 1, 2, 3 and 4 h, and transcripts for UPR-related targets and immunoglobulin heavy (μ and γ) and light (λ and κ) chains were quantified. The high quality of our data set was confirmed by analysis of housekeeping genes and three technical replicates for each biological sample. Refer to Fig. 1b for experimental design and Fig. 1c for canonical representation of UPR elements.

Heat-maps (Fig. 2) of the mRNA levels, expressed as a ratio of treated/untreated (in log base 2 scale), showed a dynamic response to ER stress by all three cell lineages, whereby some genes showed down- or up-regulation starting as early as 1 h upon challenge. Changes were considered significant if the *P*-value was ≤ 0·05 in at least two time-points or ≤ 0·01 at one time-point.

Most UPR-related genes were down-regulated, and more so in CVID patients than the healthy control. Patient P2 presented the most intense down-regulation after ER stressors treatment for all UPR-related genes, but *Hspa5* after treatment with Tm and all UPR genes but *Hspa5* and *Grp94* after Tg treatment (Fig. 2 and Supporting information, Table S3). Patient P1 had a less intense response when compared to patient P2, but also down-regulated most UPR-genes, except for genes *Calr*, *Dr5*, *Erdj3*, *Grp94*, *Ire1a*, *Rtcb* (RNA 2';3'-cyclic phosphate and 5'-OH ligase) and *Sil1* after Tg treatment. In contrast, only *Hspa5* and *Xbp1* were significantly down-regulated ($P \leq 0{\cdot}01$) after Tm treatment (Fig. 2 and Supporting information, Table S3).

Healthy donor cells down-regulated only *Hspa5*, *Chop* and *Ire1a* after Tg treatment. Tg treatment caused significant upregulation ($P \leq 0{\cdot}01$) of *Erdj3*. Tm treatment appeared to have broader effects with significant decrease in all UPR genes, but *Dr5*, *Edem1*, *Grp94*, *Ire1a*, *Rtcb* and *Sil1* in healthy cells (Fig. 2 and Supporting information, Table S3).

13652249, 2020, 1, Downloaded from https://onlinelibrary.wiley.com/doi/10.1111/cei.13410 by Universiteitsbibliotheek, Wiley Online Library on [04/08/2025]. See the Terms and Conditions (https://onlinelibrary.wiley.com/terms-and-conditions) on Wiley Online Library for rules of use; OA articles are governed by the applicable Creative Commons License

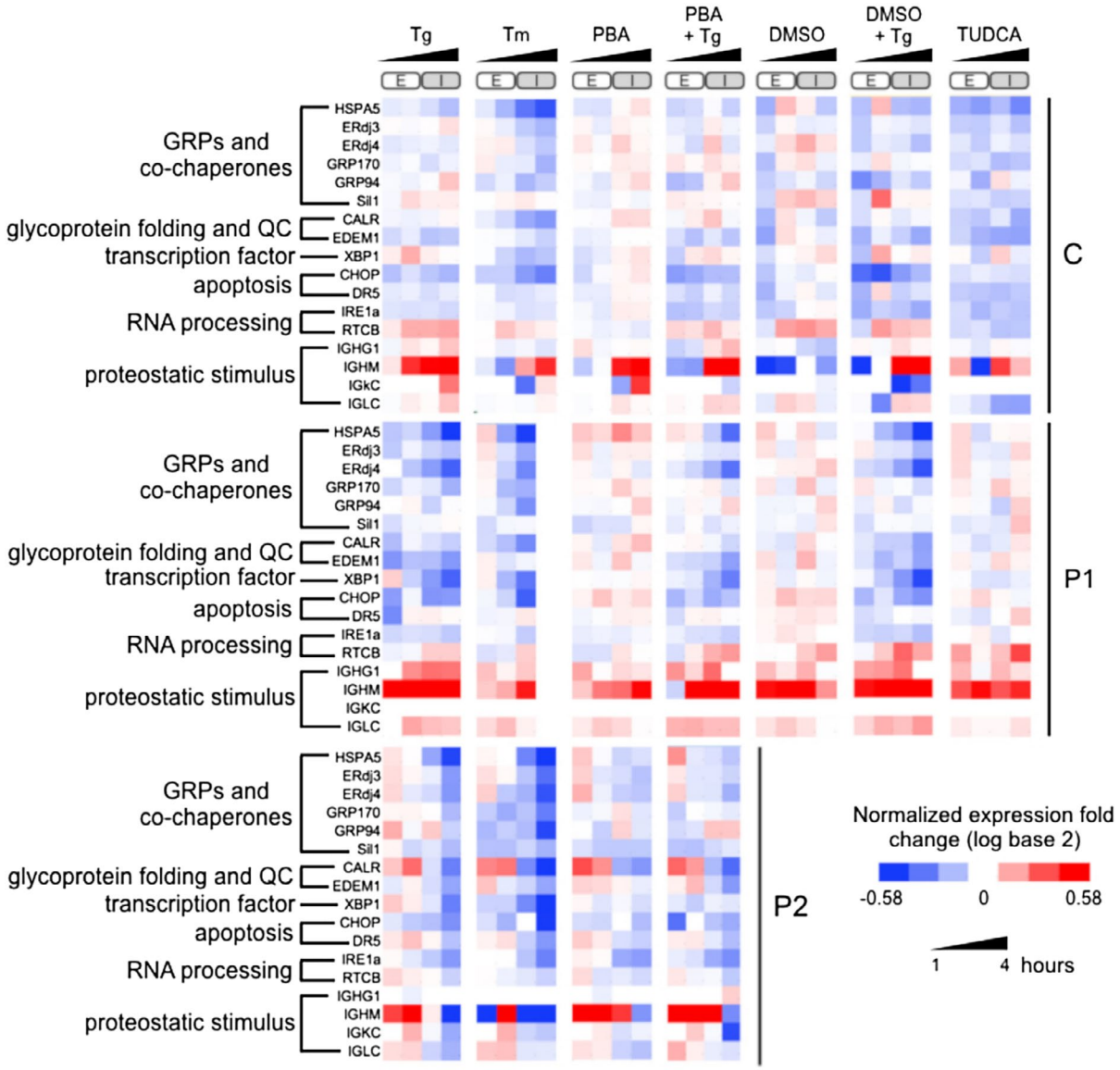

Fig. 2. Differential regulation of unfolded protein response (UPR) genes upon endoplasmic reticulum (ER) and chemical chaperones treatment. Relative changes in RNA abundance expressed as a ratio of treated/untreated [in log base 2 scale) for 17 genes (rows) in biological triplicates and technical triplicates after 1, 2, 3 and 4 h of thapsigargin (Tg) or tunicamycin (Tm)], in the presence or absence of chaperones 4-phenylbutyrate (4-PBA), dimethylsulfoxide (DMSO) or tauroursodeoxycholic acid (TUDCA). Time-points are labeled 'E' (early) and 'I' (intermediate).

When used without the ER stressors, all chaperones (4-PBA, DMSO and TUDCA) had little effect on expression of UPR-related genes when compared to untreated cells (Fig. 2 and Supporting information, Table S3). A significant effect was observed only in the up-regulation of *Calr* and *Grp94* in healthy cells (Fig. 2 and Supporting information, Table S3). In patient P2 cells, 4-PBA caused significant down-expression of genes *Chop*, *Erdj4*, *Sil1* and *Xbp1* when compared to untreated cells. It caused up-regulation of *Dr5* ($P \leq 0{\cdot}01$). *Calr* presented up-regulation during the first 2 h under 4-PBA, followed by down-regulation. No significant effects were observed with DMSO alone in both healthy and patients' cells (Fig. 2 and Supporting information, Table S3). For TUDCA alone, significant down-regulation was observed in healthy cells with all UPR-related genes but *Chop*, *Rtcb*, *Sil1* and *Xbp1* (Fig. 2 and Supporting information, Table S3). Only *Xbp1* was significantly down-regulated in patient P1 cells treated with TUDCA. TUDCA caused increased expression ($P \leq 0{\cdot}01$) of *Rtcb* and *Sil1* in patient P1. DMSO and TUDCA treatments, alone or in combination with Tg, were not performed in patient P2 due to insufficient cell yields.

13652249, 2020, 1, Downloaded from https://onlinelibrary.wiley.com/doi/10.1111/cei.13410 by Universiteitsbibliotheek, Wiley Online Library on [04/08/2025]. See the Terms and Conditions (https://onlinelibrary.wiley.com/terms-and-conditions) on Wiley Online Library for rules of use; OA articles are governed by the applicable Creative Commons License

When associated with ER stressor Tg, 4-PBA dampened both down- and up-regulation of UPR targets caused by the stressor (Fig. 2 and Supporting information, Table S3). Significant decreases were found for *Chop*, *Dr5*, *Edem1*, *Erdj3* and *Ire1a* in healthy cells. We also observed up-regulation of *Calr* at 3 h ($P \leq 0{\cdot}01$). In patient P1 cells, 4-PBA dampened down-regulation caused by Tg of *Hspa5*, *Chop*, *Edem1* and *Xbp1*. For patient P2 cells, the presence of 4-PBA dampened down-regulation of most UPR targets ($P \leq 0{\cdot}01$), except *Hspa5*, *Grp170*, *Grp94* and *Rtcb*.

When in combination with Tg, DMSO affected the expression of more genes in patient P1 compared to healthy cells (Fig. 2 and Supporting information, Table S3). In healthy cells, the presence of DMSO and Tg increased down-regulation significantly for *Hspa5*, *Chop*, *Dr5*, *Edem1* and *Ire1a* genes. *Sil1* increased expression ($P \leq 0{\cdot}01$) under DMSO and Tg association. In patient P1 cells, the presence of DMSO increased the response to Tg: *Hspa5*, *Calr*, *Chop*, *Edem1*, *Erdj3*, *Erdj4*, *Grp94*, *Ire1a* and *Xbp1* were down-regulated significantly ($P \leq 0{\cdot}01$).

Among all experimental conditions tested, the presence of ER stressors and/or chaperones was associated with increased expression of immunoglobulin μ heavy chain (*Ighm*). The only exceptions were observed with DMSO alone in healthy cells and Tm in patient P2 cells, where we observed a tendency, but no significant change.

Extreme down-regulation of *Hspa5* and *Xbp1* in CVID cells during early phase of UPR

Chaperone *Hspa5*, transcription factor *Xbp1* and immunoglobulin heavy chain μ (*Ighm*) were the genes most intensely affected in our experimental setup. *Hspa5* and *Xbp1* suffered considerable down-regulation in the initial hours upon ER stress, regardless if induced by Tg or Tm (Fig. 3a for Tg and 3B for Tm, left and middle panels). Patients P1 (Fig. 3a, gray bars) and P2 (Fig. 3a, black bars) showed stronger inhibition of *Hspa5* and *Xbp1*, reaching −1·6- and −1·4-folds for *Hspa5*, and −1·4and −1·3folds for *Xbp1*, respectively, after 4 h of ER stress caused by Tg.

Patient P2 was the most responsive cell line to Tm, presenting the strongest inhibition of transcription of *Hspa5* (−2-fold), *Xbp1* (−1·5-fold) and *Ighm* (−54-fold) in response to 4 h of treatment with this ER stressor (Fig. 3b, black bars).

Expression of *Ighm* (μ heavy chain of immunoglobulin) seemed to be unaffected by ER stressors in healthy (black bar) and P1 (gray bar) cells (Fig. 3a, right panels and Supporting information, Fig. S2c). Expression of *Ighm* in patient P2 (Fig. 3a, right panel, black bar) was down-regulated in all treatments. The highest levels of inhibition were found when these cells were stressed with Tm (Fig. 3b, right panel, black bar). Patient P2 presented the highest expression of *Ighm* in the initial hours after Tg, Tm, 4-PBA and Tg + 4-PBA treatments, peaking at 2 h, but followed by a rapid decrease in transcripts levels (Supporting information, Fig. S2c). For the complete time–course on *Hspa5*, *Xbp1* and *Ighm* refer to Supporting information, Fig. S2.

Discussion

Building highly accurate and quantitative regulatory networks in mammals pose large challenges due mainly to complexity of the regulatory logic and technical limitations

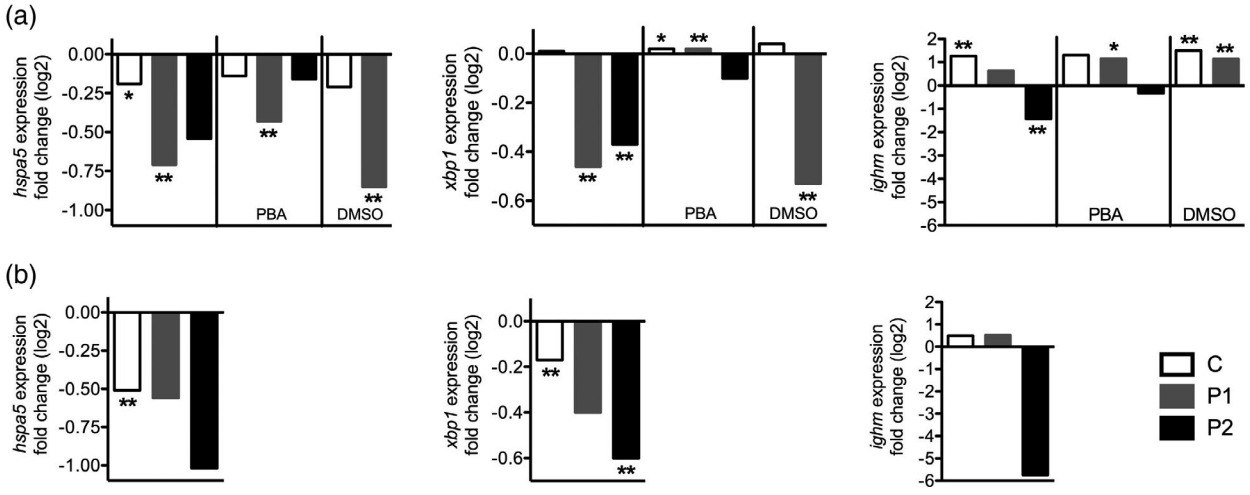

Fig. 3. Down-regulation of *Hspa5* and *Xbp1* during UPR. *Hspa5* (left panels), *Xbp1* (middle panels) and *Ighm* (right panels) RNA abundance expressed as a ratio of treated/untreated (in log base 2 scale) at 4 h after treatment with thapsigargin (a) or tunicamycin (b) in the presence or absence of chaperones [4-phenylbutyrate (4-PBA) or dimethylsulfoxide (DMSO)] of Epstein–Barr virus (EBV)-B cells from a healthy donor (c, black bars) and two common variable immunodeficiency (CVID) patients (P1 and P2, red and blue bars, respectively). $^{*}P \leq 0{\cdot}05$, $^{**}P \leq 0{\cdot}01$. For complete time–courses and *P*-values refer to Supporting information, Fig. S2 and Table S3, respectively.

13652249, 2020, 1, Downloaded from https://onlinelibrary.wiley.com/doi/10.1111/cei.13410 by Universiteitsbibliotheek, Wiley Online Library on [04/08/2025]. See the Terms and Conditions (https://onlinelibrary.wiley.com/terms-and-conditions) on Wiley Online Library for rules of use; OA articles are governed by the applicable Creative Commons License

in manipulation of mammalian systems [43,44]. Here we used high-quality measurement of mRNA expression levels of key UPR and immunoglobulin genes. Importantly, the measurements were performed in B cells derived from a healthy subject and CVID patients, providing an important data set from a model as close to the clinical phenotype as possible.

We mapped the results to the signaling network for the UPR (Fig. 4). Unexpectedly, they revealed an early inhibition of UPR in all cells, which was even more extreme in patient cells. Treatment with chemical chaperones reversed the early inhibition and activated the UPR in both patient and healthy cells, suggesting that chemical chaperones might be of value in helping hypogammaglobulinemic patients fold

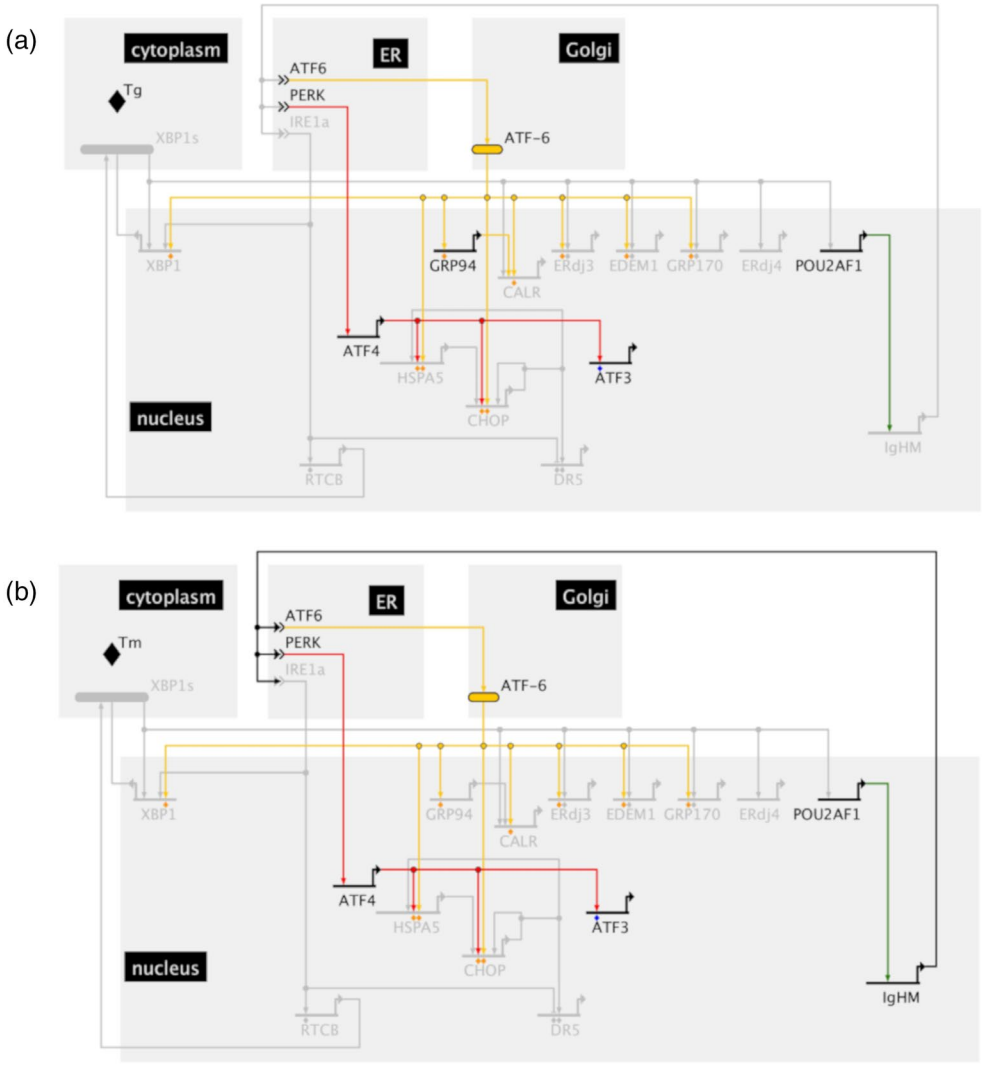

Fig. 4. Putative regulatory networks for the unfolded protein response in mature human B cells, 4 h after endoplasmic reticulum (ER) stress and/or chemical chaperones treatment. These regulatory circuits were inferred from the gene expression data and consider only immunoglobulin (Ig)M as proteostatic stimulus. Inputs and outputs of indicated genes are color coded according to their upstream origin [yellow for activating transcription factor 6 (ATF6), red for eukaryotic translation initiation factor 2-alpha kinase 3 (PERK), blue for serine/threonine-protein kinase/endoribonuclease (IRE1α) and green for spliced X-box binding protein 1 (sXBP1)]. Orange lines indicate those elements whose expression depends on inputs from both ATF6 (yellow) and PERK (red) pathways. Linkages substantiated by *cis*-regulatory data from literature are indicated by diamonds colored according to strength of the experimental evidence: blue diamonds for expression studies using gain/loss of function, pink diamonds for binding affinity assays and orange diamonds for promoter analysis *in vivo*. A green bar represents post-transcriptional modification of *Xbp1* mRNA. A yellow bar represents post-translational modification of ATF6 protein. # (OR) and & (AND) are Boolean rules governing input elements in specific promoters. Bold gene = active expression. Bold gene + thick line = up-regulated expression compared to untreated control. Gray gene + gray line = down-regulated expression compared to untreated control. (a–g) Regulatory networks for the unfolded protein response (UPR) in mature human B cells (patients average minus healthy control) at 4 h after ER stress with Tg (a), Tm (b), in the presence 4-PBA [c,d (Tg+PBA)], dimethylsulfoxide [DMSO) (e,f) (Tg+DMSO)] or tauroursodeoxycholic acid (TUDCA)(g), according to experimental data from this study.

13652249, 2020, 1, Downloaded from https://onlinelibrary.wiley.com/doi/10.1111/cei.13410 by Universiteitsbibliotheek, Wiley Online Library on [04/08/2025]. See the Terms and Conditions (https://onlinelibrary.wiley.com/terms-and-conditions) on Wiley Online Library for rules of use; OA articles are governed by the applicable Creative Commons License

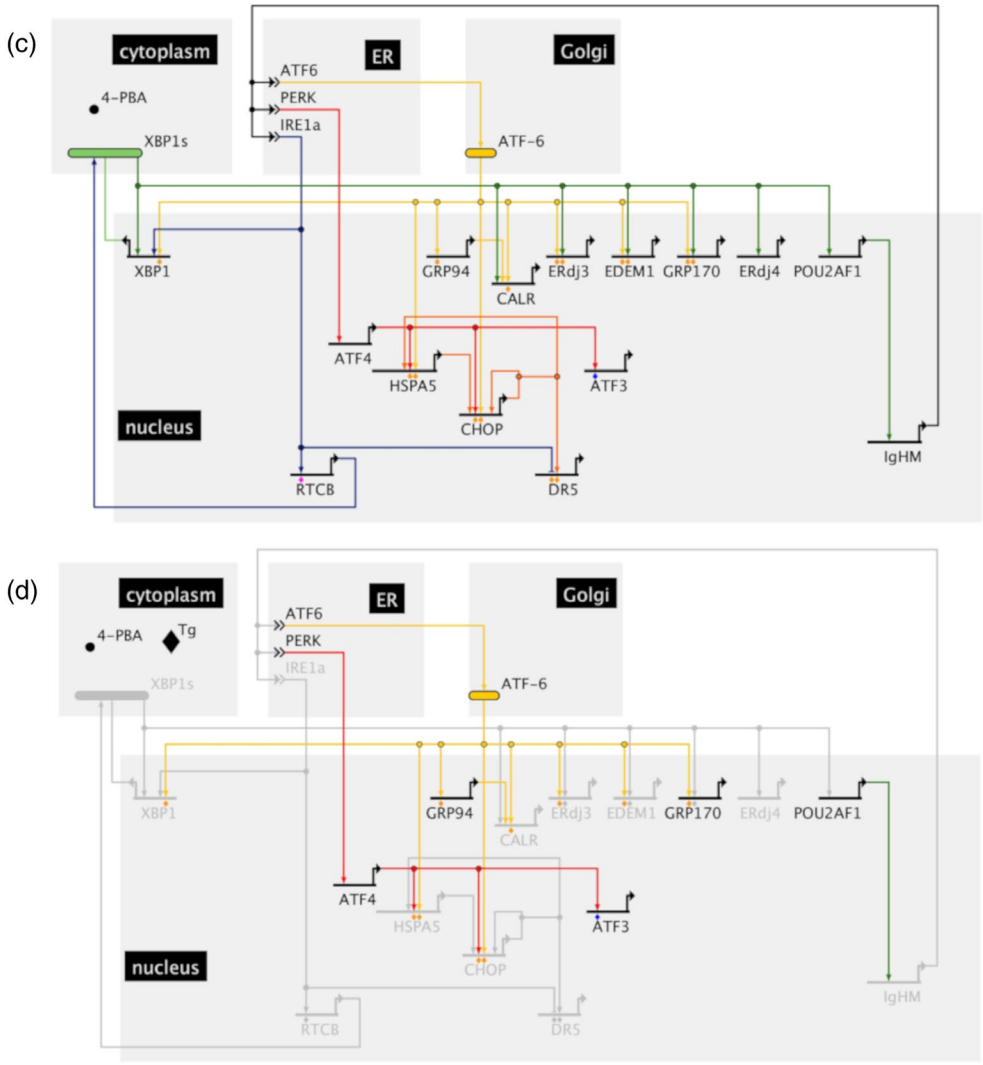

Fig. 4. Continued

their own immunoglobulins and preventing the deleterious effects of a chronically overloaded ER.

Further, we examined the possibly delayed activation of the UPR in B cells from a CVID patient, as reported by previous studies [29]. Delayed UPR in that patient resulted in an accumulation of unfolded immunoglobulin chains in the ER and failure at secreting properly folded IgM. However, what the mechanisms behind such delayed UPR activation were and how common and reversible the defect is among patients with CVID remained unknown.

To investigate the generality of this delayed UPR activation, we examined a new pair of CVID patients (P1 and P2) and a control subject (C). Both P1 and P2 presented low levels of serum IgM and IgG, but none of the described mutations involved in CVID pathogenesis [Cunningham-Rundles, unpublished; [45,46]). Besides the hallmark low levels of serum immunoglobulins, the clinical symptoms were somewhat divergent between the patients, as it is commonly seen in CVID patients (Supporting information, Table S1).

B cells from both CVID patients had a slower rate of proliferation when compared to B cells from a healthy donor (Supporting information, Fig. S1a), similarly to what we observed previously [29]. Immortalization of B cells by infection with EBV did not disrupt the ability of these cells to translate and export IgM to the cell's surface (Fig. 1a). Both patients presented lower levels of serum IgG and IgM at the time of CVID diagnosis despite presenting numbers of circulating B cells within the normal range (Supporting information, Table S1). These results indicate that immortalization by EBV infection did not change the phenotype of CVID patients' B cells, which remained capable of expressing IgM in the cell surface.

13652249, 2020, 1, Downloaded from https://onlinelibrary.wiley.com/doi/10.1111/cei.13410 by Universiteitsbibliotheek, Wiley Online Library on [04/08/2025]. See the Terms and Conditions (https://onlinelibrary.wiley.com/terms-and-conditions) on Wiley Online Library for rules of use; OA articles are governed by the applicable Creative Commons License

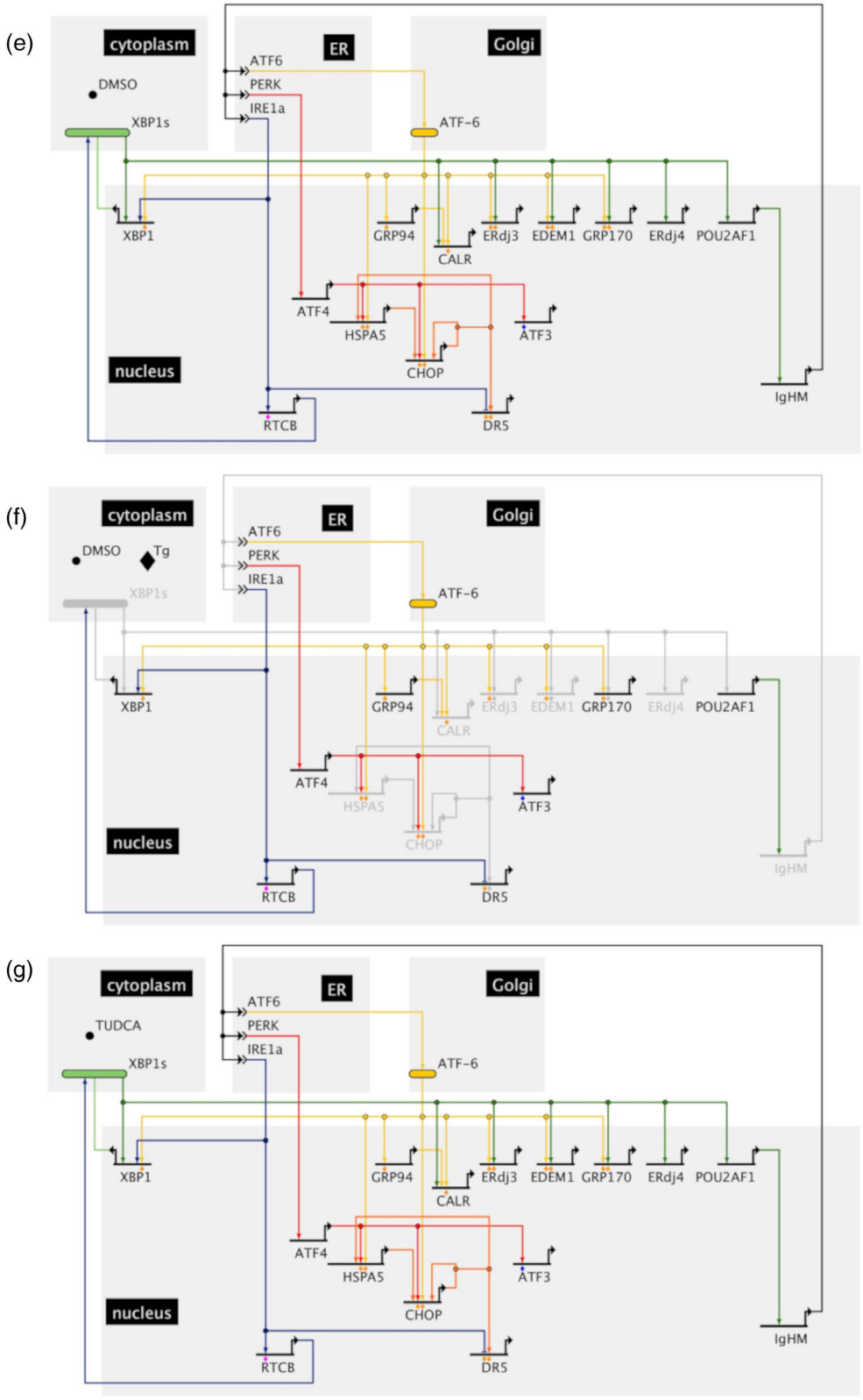

Fig. 4. Continued

13652249, 2020, 1, Downloaded from https://onlinelibrary.wiley.com/doi/10.1111/cei.13410 by Universiteitsbibliotheek, Wiley Online Library on [04/08/2025]. See the Terms and Conditions (https://onlinelibrary.wiley.com/terms-and-conditions) on Wiley Online Library for rules of use; OA articles are governed by the applicable Creative Commons License

One drawback of our experimental set-up is the fact that we immortalized B cells with EBV to yield workable numbers of B cells from CVID patients. Immortalized cells are intrinsically more resistant to stress than primary cells, and several viruses have been shown to modulate the PERK branch of UPR in mammalian cells, including EBV itself [47–50]. However, comparison with a healthy control should account for such biases. Furthermore, *Xbp1* mRNA splicing is considered a reporter for the level of ER stress [51]. *Xbp1* mRNA splicing was not detected by RT–PCR in the absence of exogenous stress in cells from both patients (Supporting information, Fig. S1b). This suggests that IRE1α is not chronically activated in these cells under untreated conditions.

Our most unexpected finding was the down-regulation of several UPR targets as early as 1 h after treatment with ER stressors (Figs 2 and 3, Supporting information, Fig. S2 and Table S3). Such repression was observed across all three cell lines, but showed stronger intensity in the cell lines derived from CVID patients. To our knowledge, only one other data set on UPR targets have found similar results at the RNA levels and showed down-regulation of the PERK branch and of overall ER stress-related components in HeLa cells between 1 and 16 h after treatment with 2·5 mM dithiothreitol (DTT) [52,53].

Up-regulation of UPR targets marks activation of the UPR [8,10]. However, these studies focused on later time-points of the response, starting measurements 6–8 h after ER stress, contrasting with our study. It is possible that cells present an initial down-regulation of UPR targets in the initial hours of response, recovering (or not) their expression at later time-points. Inability to recover from initial down-regulation of the UPR might be a pathogenesis mechanism in some CVID patients or even in other diseases.

Figure 4 and Supporting information, Movies (GIF files) show the regulatory circuits generated by the patients' experimental data. They provide novel predictions to be further explored in CVID patients. Notably, despite observed down-regulation of UPR genes, housekeeping and *Ighm* genes remained active under ER stress. Patient P1 transcribed most UPR targets in the presence of exogenous chaperones (Fig. 2 and Supporting information, Movies Q, S and U), suggesting that overall transcriptional regulation is intact.

Similarly, patient P2 increased significantly ($P \leq 0{\cdot}01$) the expression of *Calr* and *Dr5* in the initial 2 h of Tg stress (Fig. 2 and Supporting information, Movie V). However, *Sil1*, *Grp170* and *Chop* were consistently *off* in all treatments in this patient (Fig. 2 and Supporting information, Movies V–Y). This finding suggests inactive promoter regions or insufficient ATF6, their activator. Consistently, PBA increased expression of ATF6 targets (*Chop* and *Calr*) in patient P1 but not in P2 (Fig. 2, and Supporting information, Movies Q and X, respectively).

Further, patient P2 did not display *Xbp1* splicing, even after extreme stress caused by DTT (Supporting information, Fig. S1b). As XBP1 is an early master regulator of the UPR, it is conceivable that patient P2 fails to splice *Xbp1* mRNA which, in consequence, down-regulates expression of several compartments of the UPR. Transcription of immunoglobulin chains is also down-regulated in this patient (Figs 2 and 3, and Supporting information, Fig. S2c), perhaps as a last attempt of the cell to prevent protein overload into an unresponsive ER.

We show the canonical regulatory circuit that underlies the UPR in mammalian cells in Fig. 1c. Information within each cell flows from the upper left corner towards the lower right corner of the chart [41,54]. The circuit was inferred from literature that provided experimental evidence for interactions between individual genes/proteins during the UPR, focuses on genes in our study and includes only IgM as proteostatic stimulus for clarity.

Next we showed the modified circuit as derived from each sample's data in Fig. 4 for average (patients minus control) and Supporting information, Movies for complete time–courses of individual cell lines and treatments. Our data show that upon ER stress induced by drugs Tg or Tm, the number of UPR genes down-regulated in B cells from CVID patients is larger than those down-regulated in the healthy control (Fig. 4a,b; Supporting information, Movies A, B, H and I). This finding suggests that early and intense down-regulation of UPR genes in the patients' cells might contribute to insufficient immunoglobulin folding and export at later time-points.

A striking finding from these regulatory circuits is that some genes are *off* regardless of their upstream element being *on*: in both CVID patients' cells, *Calr* and *Erdj3* are *off* (Supporting information, Movies O–Y), indicating possible negative regulatory element(s). The patients could over-express such negative regulatory element(s) as the mechanism behind their early down-regulation of the UPR.

Further, we found that all tested chemical chaperones (4-PBA, DMSO and especially TUDCA) had a positive impact on expression of *Ighm* (IgM heavy chain) (Figs 2 and 3, Supporting information, Fig. S2c). This finding is new, and points to a potential use of these chemical chaperones for treatment of a subgroup of CVID patients, namely those with UPR abnormalities.

In sum, published findings and our new findings support early down-regulation of the UPR in some patients [29,55], caused probably by non-lethal defects of the UPR. Such a non-lethal defect was recently described for SEC61A1 in B cells from patients with primary hypogammaglobulinemia [56]. In comparison, our regulatory circuits point to disturbances in the ATF6 branch, and to the existence of not-yet-identified negative regulators of calreticulin and ERdj3. These findings suggest that a subgroup of hypogammaglobulinemia patients shows a delayed transcriptional

13652249, 2020, 1, Downloaded from https://onlinelibrary.wiley.com/doi/10.1111/cei.13410 by Universiteitsbibliotheek, Wiley Online Library on [04/08/2025]. See the Terms and Conditions (https://onlinelibrary.wiley.com/terms-and-conditions) on Wiley Online Library for rules of use; OA articles are governed by the applicable Creative Commons License

response to ER stress, resulting in failure to homeostasis and subsequent immunoglobulin secretion, providing new insights into the molecular basis of the disease.

Acknowledgements

This study was funded by the Brazilian National Council for Scientific and Technological Development (400662/2014-0 for R. C. S. and 309041/2012-0 for M. M. d. C.) and São Paulo State Research Foundation (11/51778-6, 12/04657-1, and 17/06289-3 for M. M. d. C.). D. B. received a FSDIE Scholarship (France). C. V. acknowledges funding by the US National Institute for Health (1R01GM113237-01 and 1R35GM127089-01). We thank Ethan Hartman for help in the initial phase of this study; Tomoko Sekiya, Fábio Mury, Marlene Lunardi and Carlos Brancato for help with Open Array technology and QuantStudio software; Roxanne Hatanaka for lending a Qubit fluorometer; Professor Dr José Krieger and Clarice Camargo for providing full-access to a QuantStudio 12K Flex Real-Time PCR System; Dr William Longabaugh for critical input using BioTapestry; Dr Luiza Guilherme for kindly providing healthy donor cells, Professor Dr Gokhan Hotamisligil for providing 4-PBA and TUDCA and late Professor Dr Eric Davidson for critical input on earlier ideas on this study. We thank Drs Fernanda Ortis and Luiza Guilherme for critical reading of this manuscript.

Disclosures

The authors declare no personal, professional or financial relationships that could potentially be construed as a conflict of interest.

Author contributions

M. M. d. C. conceived and designed the study; M. M. d. C., R. P., M. M. and D. B. conducted the experiments; D. B. and M. M. d. C. built the networks; C. V. and M. M. d. C. analyzed the arrays data; C. C.-R. recruited CVID patients and acquired clinical data; D. B., S. M., R. S., C. C.-R., C. V. and M. M. d. C. wrote the manuscript with input from all the authors.

References

1 Gass JN, Gunn KE, Sriburi R, Brewer JW. Stressed-out B cells? Plasma-cell differentiation and the unfolded protein response. Trends Immunol 2004; **25**:17–24.

2 Bettigole SE, Glimcher LH. Endoplasmic reticulum stress in immunity. Annu Rev Immunol 2015; **33**:107–38.

3 Okada T, Yoshida H, Akazawa R, Negishi M, Mori K. Distinct roles of activating transcription factor 6 (ATF6) and double-stranded RNA-activated protein kinase-like endoplasmic reticulum kinase (PERK) in transcription during the mammalian unfolded protein response. Biochem J 2002; **366**:585–94.

4 Pobre KFR, Poet GJ, Hendershot LM. The endoplasmic reticulum (ER) chaperone BiP is a master regulator of ER functions: getting by with a little help from ERdj friends. J Biol Chem 2019; **294**:2098–108.

5 Lu M, Lawrence DA, Marsters S *et al.* Opposing unfolded-protein-response signals converge on death receptor 5 to control apoptosis. Science 2014; **345**:98–101.

6 Hughes D, Mallucci GR. The unfolded protein response in neurodegenerative disorders – therapeutic modulation of the PERK pathway. FEBS J 2019; **286**:342–55.

7 Gass JN, Gifford NM, Brewer JW. Activation of an unfolded protein response during differentiation of antibody-secreting B cells. J Biol Chem 2002; **277**:49047–54.

8 Shaffer AL, Shapiro-Shelef M, Iwakoshi NN *et al.* XBP1, downstream of Blimp-1, expands the secretory apparatus and other organelles, and increases protein synthesis in plasma cell differentiation. Immunity 2004; **21**:81–93.

9 Skalet AH, Isler JA, King LB, Harding HP, Ron D, Monroe JG. Rapid B cell receptor-induced unfolded protein response in nonsecretory B cells correlates with Pro- *versus* antiapoptotic cell fate. J Biol Chem 2005; **280**:39762–71.

10 Iwakoshi NN, Lee A-H, Vallabhajosyula P, Otipoby KL, Rajewsky K, Glimcher LH. Plasma cell differentiation and the unfolded protein response intersect at the transcription factor XBP-1. Nat Immunol 2003; **4**:321–9.

11 van Anken E, Romijn EP, Maggioni C *et al.* Sequential waves of functionally related proteins are expressed when B cells prepare for antibody secretion. Immunity 2003; **18**:243–53.

12 Haas IG, Wabl M. Immunoglobulin heavy chain binding protein. Nature 1983; **306**:387–9.

13 Hendershot L. Assembly and secretion of heavy chains that do not associate posttranslationally with immunoglobulin heavy chain-binding protein. J Cell Biol 1987; **104**:761–7.

14 Melnick J, Aviel S, Argon Y. The endoplasmic reticulum stress protein GRP94, in addition to BiP, associates with unassembled immunoglobulin chains. J Biol Chem 1992; **267**:21303–6.

15 Lin HY, Masso-Welch P, Di YP, Cai JW, Shen JW, Subjeck JR. The 170-kDa glucose-regulated stress protein is an endoplasmic reticulum protein that binds immunoglobulin. Mol Biol Cell 1993; **4**:1109–19.

16 Shen Y, Hendershot LM. ERdj3, a stress-inducible endoplasmic reticulum DnaJ homologue, serves as a coFactor for BiP's interactions with unfolded substrates. Mol Biol Cell 2005; **16**:40–50.

17 Reimold AM, Iwakoshi NN, Manis J *et al.* Plasma cell differentiation requires the transcription factor XBP-1. Nature 2001; **412**:300–7.

18 Chapel H, Cunningham-Rundles C. Update in understanding common variable immunodeficiency disorders (CVIDs) and the management of patients with these conditions. Br J Haematol 2009; **145**:709–27.

13652249, 2020, 1, Downloaded from https://onlinelibrary.wiley.com/doi/10.1111/cei.13410 by Universiteitsbibliotheek, Wiley Online Library on [04/08/2025]. See the Terms and Conditions (https://onlinelibrary.wiley.com/terms-and-conditions) on Wiley Online Library for rules of use; OA articles are governed by the applicable Creative Commons License

19 Ameratunga R. Assessing disease severity in common variable immunodeficiency disorders (CVID) and CVID-like disorders. Front Immunol 2018; **9**:2130.

20 Selenius JS, Martelius T, Pikkarainen S *et al*. Unexpectedly high prevalence of common variable immunodeficiency in Finland. Front Immunol 2017; **8**:1190.

21 Grimbacher B, Hutloff A, Schlesier M *et al*. Homozygous loss of ICOS is associated with adult-onset common variable immunodeficiency. Nat Immunol 2003; **4**:261–8.

22 Salzer U, Chapel HM, Webster ADB *et al*. Mutations in TNFRSF13B encoding TACI are associated with common variable immunodeficiency in humans. Nat Genet 2005; **37**:820–8.

23 van Zelm MC, Reisli I, van der Burg M *et al*. An antibody-deficiency syndrome due to mutations in the *CD19* gene. N Engl J Med 2006; **354**:1901–12.

24 Warnatz K, Salzer U, Rizzi M *et al*. B-cell activating factor receptor deficiency is associated with an adult-onset antibody deficiency syndrome in humans. Proc Natl Acad Sci USA 2009; **106**:13945–50.

25 Kuijpers TW, Bende RJ, Baars PA *et al*. CD20 deficiency in humans results in impaired T cell–independent antibody responses. J Clin Invest 2010; **120**:214–22.

26 van Zelm MC, Smet J, Adams B *et al*. CD81 gene defect in humans disrupts CD19 complex formation and leads to antibody deficiency. J Clin Invest 2010; **120**:1265–74.

27 Salzer U, Warnatz K, Peter H. Common variable immunodeficiency – an update. Arthritis Res Ther 2012; **14**:223.

28 de Valles-Ibáñez G, Esteve-Solé A, Piquer M *et al*. Evaluating the genetics of common variable immunodeficiency: monogenetic model and beyond. Front Immunol 2018; **9**:636.

29 Kuribayashi JS, Bombardieri CR, Baracho GV *et al*. Slower rescue of ER homeostasis by the unfolded protein response pathway associated with common variable immunodeficiency. Mol Immunol 2008; **45**:2990–7.

30 Treiman M, Caspersen C, Christensen SB. A tool coming of age: thapsigargin as an inhibitor of sarco-endoplasmic reticulum Ca(2+)-ATPases. Trends Pharmacol Sci 1998; **19**:131–5.

31 Lehrman MA. Oligosaccharide-based information in endoplasmic reticulum quality control and other biological systems. J Biol Chem 2001; **276**:8623–6.

32 Cetin M, Eser B, Er O *et al*. Effects of DMSO on platelet functions and P-selectin expression during storage. Transfus Apheresis Sci 2001; **24**:261–7.

33 Shuster R, Traub-Dargatz J, Baxter G. Survey of diplomates of the American College of Veterinary Internal Medicine and the American College of Veterinary Surgeons regarding clinical aspects and treatment of endotoxemia in horses. J Am Vet Med Assoc 1997; **210**:87–92.

34 Ozcan U. Chemical chaperones reduce ER stress and restore glucose homeostasis in a mouse model of type 2 diabetes. Science 2006; **313**:1137–40.

35 Cuadrado-Tejedor M, Garcia-Osta A, Ricobaraza A, Oyarzabal J, Franco R. Defining the mechanism of action of 4-phenylbutyrate to develop a small-molecule-based therapy for Alzheimers disease. Curr Med Chem 2011; **18**:5545–53.

36 Zhou W, Bercury K, Cummiskey J, Luong N, Lebin J, Freed CR. Phenylbutyrate up-regulates the DJ-1 protein and protects neurons in cell culture and in animal models of Parkinson disease. J Biol Chem 2011; **286**:14941–51.

37 Solá S, Castro RE, Laires PA, Steer CJ, Rodrigues CMP. Tauro-ursodeoxycholic acid prevents amyloid-beta peptide-induced neuronal death via a phosphatidylinositol 3-kinase-dependent signaling pathway. Mol Med (Cambridge, MA) 2003; **9**:226–34.

38 Schoemaker MH, Conde de la Rosa L, Buist-Homan M *et al*. Tauroursodeoxycholic acid protects rat hepatocytes from bile acid-induced apoptosis via activation of survival pathways. Hepatology 2004; **39**:1563–73.

39 Carey EJ, Ali AH, Lindor KD. Primary biliary cirrhosis. Lancet 2015; **386**:1565–75.

40 Tosato G, Cohen JI. Generation of Epstein–Barr virus (EBV)-immortalized B cell lines. In: Coligan JE, Bierer BE, Margulies DH, Shevach EM, Strober W, eds. Current protocols in immunology. Hoboken, NJ, USA: John Wiley & Sons Inc., 2007:im0722s76.

41 Longabaugh WJR, Davidson EH, Bolouri H. Visualization, documentation, analysis, and communication of large-scale gene regulatory networks. Biochim Biophys Acta 2009; **1789**:363–74.

42 Paquette SM, Leinonen K, Longabaugh WJR. BioTapestry now provides a web application and improved drawing and layout tools. F1000Research 2016; **5**:39.

43 Kim HD, Shay T, O'Shea EK, Regev A. Transcriptional regulatory circuits: predicting numbers from alphabets. Science 2009; **325**:429–32.

44 Amit I, Regev A, Hacohen N. Strategies to discover regulatory circuits of the mammalian immune system. Nat Rev Immunol 2011; **11**:873–80.

45 Farmer JR, Ong M-S, Barmettler S *et al*. Common variable immunodeficiency non-infectious disease endotypes redefined using unbiased network clustering in large electronic datasets. Front Immunol 2018; **8**:1740.

46 Smith T, Cunningham-Rundles C. Primary B-cell immunodeficiencies. Hum Immunol 2019; **80**:351–62.

47 Isler JA, Skalet AH, Alwine JC. Human cytomegalovirus infection activates and regulates the unfolded protein response. J Virol 2005; **79**:6890–9.

48 Lee DY, Sugden B. The LMP1 oncogene of EBV activates PERK and the unfolded protein response to drive its own synthesis. Blood 2008; **111**:2280–9.

49 Liu J, HuangFu W-C, Kumar KGS *et al*. Virus-induced unfolded protein response attenuates antiviral defenses via phosphorylation-dependent degradation of the Type i interferon receptor. Cell Host Microbe 2009; **5**:72–83.

50 Borsa M, Ferreira PLC, Petry A *et al*. HIV infection and antiretroviral therapy lead to unfolded protein response activation. Virol J 2015; **12**:77.

51 Marciniak SJ. CHOP induces death by promoting protein synthesis and oxidation in the stressed endoplasmic reticulum. Genes Dev 2004; **18**:3066–77.

13652249, 2020, 1, Downloaded from https://onlinelibrary.wiley.com/doi/10.1111/cei.13410 by Universiteitsbibliotheek, Wiley Online Library on [04/08/2025]. See the Terms and Conditions (https://onlinelibrary.wiley.com/terms-and-conditions) on Wiley Online Library for rules of use; OA articles are governed by the applicable Creative Commons License

52 Cheng Z, Teo G, Krueger S *et al*. Differential dynamics of the mammalian mRNA and protein expression response to misfolding stress. Mol Syst Biol 2016; **12**:855.

53 Teo G, Bin Zhang Y, Vogel C, Choi H. PECAplus: statistical analysis of time-dependent regulatory changes in dynamic single-omics and dual-omics experiments. npj Syst Biol Applic 2018; **4**:3.

54 Bolouri H, Davidson EH. Transcriptional regulatory cascades in development: initial rates, not steady state, determine network kinetics. Proc Natl Acad Sci USA 2003; **100**:9371–6.

55 Costa CZF, da Rosa SEA, de Camargo MM. The unfolded protein response: how protein folding became a restrictive aspect for innate immunity and B lymphocytes1: folding immunity-related proteins. Scand J Immunol 2011; **73**:436–48.

56 Schubert D, Klein M-C, Hassdenteufel S *et al*. Plasma cell deficiency in human subjects with heterozygous mutations in Sec61 translocon alpha 1 subunit (SEC61A1). J Allergy Clin Immunol 2018; **141**:1427–38.

Supporting Information

Additional supporting information may be found in the online version of this article at the publisher's web site:

Fig. S1. Defective *Xbp1* splicing in P2 cells, but not P1. (a) Cells quantification by BrdU incorporation over 11 days in culture without treatments. (b) *Xbp1* mRNA splicing was not detected by RT-PCR in the absence of DTT in cells from both patients. In the presence of DTT, only P1 was capable of splicing *Xbp1* mRNA

Fig. S2. Complete time-courses for *Hspa5*, *Xbp1* and *Ighm* during UPR. *Hspa5* (a), *Xbp1* (b), and *Ighm* (c) RNA abundance expressed as a ratio of Treated / Untreated (in log base 2 scale) at 1, 2, 3, and 4 hours after thapsigargin (Tg) or tunicamycin (Tm, insert box) in the presence or absence of chaperones 4-PBA, DMSO, or TUDCA in B cells from a healthy donor (C, black line) or two CVID patients (P1 and P2, red and blue lines, respectively). $^{*}P \leq 0{\cdot}05$, $^{**}P \leq 0{\cdot}01$.

Table S1. Clinical data on patients that originated the cell lineages used in this study

Table S2. TaqMan OpenArray primers for transcript quantification. Primers are custom-made by ThermoFisher. Sequences protected by patent.

Table S3. Strict quality control rules resulted in a high-confidence dataset: p values for different treatments

13652249, 2020, 1, Downloaded from https://onlinelibrary.wiley.com/doi/10.1111/cei.13410 by Universiteitsbibliotheek, Wiley Online Library on [04/08/2025]. See the Terms and Conditions (https://onlinelibrary.wiley.com/terms-and-conditions) on Wiley Online Library for rules of use; OA articles are governed by the applicable Creative Commons License